Article

Experimental and RSM-Based Process-Parameters Optimisation for Turning Operation of EN36B Steel

Ramesh Kumar [1], Ashwani Kumar [2,*], Laxmi Kant [3], Arbind Prasad [4], Sandeep Bhoi [5], Chandan Swaroop Meena [6,7,*], Varun Pratap Singh [8] and Aritra Ghosh [9,*]

[1] Department of Mechanical Engineering, Saharsa College of Engineering, Saharsa 852201, Bihar, India
[2] Technical Education Department Uttar Pradesh Kanpur, Kanpur 208024, Uttar Pradesh, India
[3] Department of Mechanical Engineering, Government Engineering College Bhojpur, Patna 800024, Bihar, India
[4] Department of Mechanical Engineering, Katihar Engineering College (under Department of Science & Technology, Government of Bihar), Katihar 854109, Bihar, India
[5] Department of Mechanical Engineering, Parala Maharaja Engineering College, Berhampur 761003, Odisha, India
[6] CSIR-Central Building Research Institute, Roorkee 247667, Uttarakhand, India
[7] Academy of Scientific and Innovative Research (AcSIR), Ghaziabad 201002, Uttar Pradesh, India
[8] Department of Mechanical Engineering, School of Engineering, University of Petroleum and Energy Studies, Dehradun 248007, Uttarakhand, India
[9] Faculty of Environment, Science and Economy (ESE), Renewable Energy, Electric and Electronic Engineering, University of Exeter, Penryn, Cornwall TR10 9FE, UK
* Correspondence: drashwanikumardte@gmail.com (A.K.); chandanswaroop2008@gmail.com (C.S.M.); a.ghosh@exeter.ac.uk (A.G.)

Abstract: The main objective of this article is to perform the turning operation on an EN36B steel work-billet with a tungsten carbide tool, to study the optimal cutting parameters and carry out an analysis of flank-wear. Experimental and simulation-based research methodology was opted in this study. Experimental results were obtained from the lab setup, and optimisation of parameters was performed using RSM (response surface methodology). Using RSM, cutting-tool flank-wear was optimised, and the cutting parameters which affect the flank wear were determined. In results main effect plot, contour plot, the surface plot for flank-wear and forces (Fx, Fy and Fz) were successfully obtained. It was concluded that tool flank-wear is affected by depth of cut, and that flank-wear generally increases linearly with increasing cutting-speed, depth of cut and feed-rate. To validate the obtained results, predicated and measured values were plotted and were in very close agreement, having an accuracy level of 96.33% to 98.92%.

Keywords: cutting-tool wear; process parameters; turning operation; optimisation; response-surface method; EN36B steel

1. Introduction

In metal cutting, tribology plays an important role, as it decides the surface quality as well as the performance of the product during operation. Wear, friction and surface roughness constitute an integral part of tribology [1–3]. Four basic elements, i.e., body, counter-body, ambient medium, and interface material make up the structure of the tribological system. The machining of the materials is an example of the open-type tribological system in which the body can be replaced by a tool, the counter-body can be replaced by work material, and the interface material can be replaced by the lubricant used for cooling purposes in the machining. One of the most commonly used techniques for the fabrication of components is machining; during the machining of components, excessive wear of the cutting tool gives rise to distortion in the dimensions of manufactured components, and increases the level of scrapped material [4,5]. Hence, it becomes necessary to monitor the cutting-tool wear. Turning is an example of the machining process, and in this process,

the extra materials on the workpiece can be removed by a single-point cutting tool [6]. The main reason for cutting-tool failure is a mechanical failure of the cutting tool, which may be due to excessive forces and shocks. The nature of this type of failure of the cutting tool is catastrophic, and hence this type of failure is detrimental. It occurs due to the intensive temperature and the stresses, which are quick to cause dulling, due to plastic deformation [7–9]. This type of failure is unwanted and detrimental, and takes place at a very fast rate. Another type of failure that occurs in the tool is gradual wear of the cutting tools, which causes failure of the flank surface and the rake surface of the tool [10–12].

The two modes of tool failure, i.e., the mechanical failure of the tool and the failure of the tool due to intensive stresses and temperature, are very harmful to the tool as well as to the job. Therefore, these types of tool failures need to be stopped by taking some necessary action, such as by using suitable tool geometry and tool materials. Furthermore, tool failure due to gradual wear is inevitable and cannot be stopped [13–15]. Gradual wear of the tool can only be slowed down, to increase the life of the tool. In the machining process, the cutting tool needs to be replaced just before the tool is going to fail or just after the tool has failed. We need criteria to judge or to decide whether a tool is about to fail or has failed [16–18]. Researchers have performed the optimisation study of cutting tools by turning for surface roughness. They have determined tool wear using force signals, as we can extract more information about the machining process from the force signals [19–23]. In recent studies, authors have studied the process parameters using RSM, which has been adopted for the current study. In the present research work, the relationship among the feed force, cutting-force components (the ratio of the force components, F_X and F_Z) flank-wear, and other cutting parameters (cutting speed, feed, depth of cut and diameter) was established by performing a series of experiments for accessing tool characteristics [24–27]. Tool-life performance, the wear mechanism, and surface roughness were also studied by Motorcu et. al., by using input parameters. They investigated the wear behaviour of a ceramic tool Al_2O_3, and, Al_2O_3 coated with TiN and CBN/TiC for the machining of the hardened steel AISI 52100, and surface roughness was compared under various conditions. Joardar et al. made an attempt to find the effect of specific cutting variables in straight-turning, on cutting forces. The materials used in the straight-turning operation were the metal matrix composites of aluminium under dry cutting conditions. Some of the influencing parameters selected are as follows: depth of cut, cutting speed, and weight percentage of SiCP [28–31].

Sikdar and Chen successfully established a relationship between the above components. They further conclude that adhesive and abrasive actions between the workpiece and the tool, cause the flank wear. First, there the flank wear starts at the tip of the cutting tool, and then it increases widthways, thus resulting in a wear land. Sun et. al. and Oraby and Hayhurst studied a model for finding tool life and wear in terms of the variation of a ratio of the force components acting at the tooltip, which were established by nonlinear regression analysis. In continuation, Noordin et. al., using RSM, studied the performance of carbide tools [32–35]. A comprehensive model that relates the wear to the change in the cutting force was proposed and tested. They describe the performances of a multilayer, tungsten carbide tool using response-surface methodology. The cutting test was performed with a constant depth of cut under dry conditions [36–40]. Yang and Tang considered a practical turning case, which could be used for tool-wear estimation when the crater-wear effect is negligible (or be combined with the crater-wear model when the crater-wear effect is influential). They showed successfully that the method which provides an efficient and systematic methodology in the optimum designing of cutting parameters is the Taguchi method. Kumar et al. studied the optimization techniques for different engineering problems. Bhoi et al. successfully carried out condition monitoring and a delamination study on dynamic analysis. They investigated the wear failure [41–44].

In the literature, authors have studied cutting-tool failures due to wear. In continuation, this article presents a tool-wear study using experimental and simulation results [45–48]. In this article, a turning operation was performed on an EN36B steel work-billet with a

tungsten carbide tool and process parameters such as the feed components of force (F_X, F_Y and F_Z), cutting speed, feed rate and depth of cut. These were studied experimentally and results were validated using the RSM tool.

2. Materials and Methodology

In the current study, we adopted the design of experiments (DOE) to plan and optimise the experiments required. A test or series of tests are called upon to solve any problem with the help of experiments, and this plays a major role in the DOE. For designing the factorial experiments, experimental trials needed to be performed with all combinations of the levels of factors. However, with the help of the DOE, there is the capability to simultaneously investigate the effects of different variables on the response, i.e., on the output variable. The experiments in the DOE consist of many tests in which input variables are altered accordingly, and the data are collected after the tests. Tool wear affects the feed components of the force (F_X) and the radial components of force (F_y). The frictional and sliding condition between the workpiece and the tool is closely related to the components of force F_X and F_Y. The respective friction condition of F_X and F_Y, and their combined effects, can be measured by F_Z. The vertical component of force, F_Z can be measured in terms of the power and torque required for the operation of the lathe.

In the initial stage, the value of the component of forces, i.e., F_X and F_Z were almost the same. After the progress of the machining operation, and due to the wear of the cutting-edge of the tool, the values of the components of the forces no longer remain the same. The values of the forces, i.e., F_X and F_Z depends on the condition of distribution of the wear-scars on the cutting-edge of the tool. Generally, on the tool flank-face, the wear scars are not distributed evenly. The nose wear (NW) of the tool is mainly responsible for the change in the value of the radial component of force, i.e., F_Y. The presence of wear on the nose and flank of the tool affects the force component, i.e., F_X. The force components associated with a particular area are mostly influenced by the domination of wear in that area. At the point where the tool has maximum projection into the workpiece, the nose-wear was measured. The flank-wear was measured at the maximum wear land on the tool flank. According to ISO, the average value of wear at failure VB (width of wear land) = 0.30 mm. The maximum value of VB is 1.7 mm, which is permissible in flank-wear (VB). Many professional uses the DOE to find the product components and process conditions that affect quality. After this, they try to find the input factors or variables that need to be regulated for obtaining the optimum point of the desired objective. The level that was chosen for each cutting parameter is given in Table 1. The parameter levels were selected as recommended by the tool manufacturer. Cutting parameters and their levels are given in Table 1. Three cutting parameters at three levels led to 27 tests. The plan of the experiments as designed using concepts of DOE is given in Table 2. A full factorial design using Minitab15 software (Academic version, 2020, India) was created, and the experiments were performed using this plan. Cutting speed, feed rate and depth of cut are the three different levels ($3^3 = 27$) for which experiments were performed. At the last stage the predicated values and measured values were compared, and the graph was plotted for the results analysis.

Table 1. Cutting parameters and their level.

S. No.	Level	Cutting Speed V (m/min)	Feed Rate f (mm/rev)	Depth of Cut d (mm)
1	Low (−1)	40	0.04	0.50
2	Medium (0)	55	0.06	0.75
3	High (1)	70	0.08	1.00

Table 2. Chemical composition of EN36B.

S. NO.	Component	Min (%)	Max (%)
1	Carbon (C)	0.10	0.160
2	Silicon(Si)	0.10	0.0035
3	Manganese (Mn)	0.35	0.60
4	Phosphorus (P)	Nil	0.04
5	Sulphur (S)	Nil	0.04
6	Chromium (Cr)	0.70	1.00
7	Nickel (Ni)	3.0	3.75

The experiments were performed using the single-point cutting tool, and the experimental setup on the lathe with the single-point cutting tool is shown in Figure 1. Figure 1a shows the tool-post of the lathe, and the complete setup of the lathe machine is shown in Figure 1b. The data-acquisition setup used for measuring the tool wear is shown in Figure 1c.

(a) **(b)** **(c)**
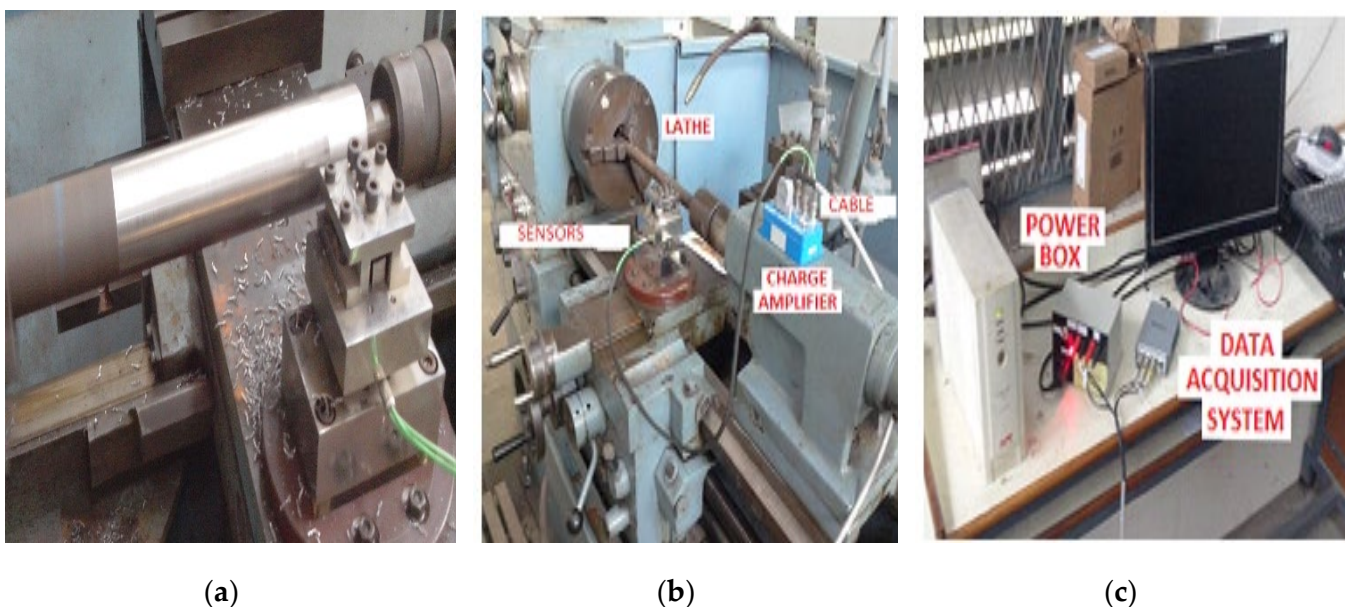
Figure 1. Experiment setup for wear analysis of tungsten carbide tool: (**a**) tool post, (**b**) different parts on the lathe, and (**c**) setup of the data-acquisition system.

In the current study, EN36B steel of dimension 50 mm × 400 mm was used as a workpiece. The purpose of selecting EN36B as a workpiece material is because of its abundance of use in manufacturing. It is generally used for manufacturing automobile components such as worm shafts, gears, spline shafts, and pinion shafts. It is also used in the manufacturing of heavy-vehicle transmission and auto components, aircraft gear mining, chuck jaws, steering worms, pinions, cogs, and gudgeon pins. The tool holder SCLCR1212F09 is used with a carbide tool insert, CCMT09T302. After performing every experiment, the insert was changed, to minimise the effect of tool wear on the material removal rate and cutting forces. A piezoelectric dynamometer (KISTLER Maker, Kistler Instruments India Pvt. Ltd., Chennai, India) was used for measuring the cutting forces.

The weight of the workpiece is precisely measured with an accuracy of up to a milligram, with the help of a precision weighing machine (MT India Pvt. Ltd., Mumbai, India). Tool wear (depth of flank-wear VB) is measured with the help of a metallurgical microscope (Delhi Metco, New Delhi, India). The chemical composition of the EN36B used for the machining process is listed in Table 2. The EN36B core strength can be up to 1230 N/mm^2, and the hardness value is 255 (Brinell hardness RC26).

3. Results and Discussion

The effect of the different design parameters on the quality of the machining process can be analysed by using the analysis of variance (ANOVA). For flank-wear, the results of the analysis of variance obtained at the 5% level of significance were analysed. The magnitude and existence of some of the physical quantities could not be quantified directly, but by using the ANOVA it was possible to find them. The ANOVA is not only able to quantify physical quantity, but can also analyse its effect. An example of this might be a force, which is neither is held nor seen. However, it can not only be detected, but also quantified, with the help of these effects, such as deformation, deflection, strain, pressure, etc., which can be quantified. The signals of these effects need to be conditioned properly, prior to analysis, for accurate, easy measurement of these effects. The values of the speed, feed and depth of cut obtained, are given in the form of an observation table in Table 3. The result of analysis of variance (ANOVA) for VB, F_X, F_Y and F_Z is tabulated in Table 4.

Table 3. Observation table obtained for cutting parameters speed, feed. and depth of cut.

| S. No	v (m/min)	f (mm/rev)	d (mm)	F_X (N)	F_Y (N)	F_Z (N)	VB (mm)
1	40	0.04	0.5	15.125	44.835	35.335	0.321
2	40	0.04	0.75	33.375	69.82	65.42	0.373
3	40	0.04	1	65.36	91.395	88.165	0.433
4	40	0.06	0.5	16.355	50.225	40.2	0.34
5	40	0.06	0.75	42.82	78.77	73.21	0.414
6	40	0.06	1	69.05	98.865	110.84	0.453
7	40	0.08	0.5	17.515	57.98	53.555	0.359
8	40	0.08	0.75	45.06	87.22	88.485	0.412
9	40	0.08	1	71.315	108.85	133.17	0.452
10	55	0.04	0.5	14.67	41.605	29.295	0.346
11	55	0.04	0.75	33.135	67.235	62.46	0.403
12	55	0.04	1	53.13	81.385	79.3	0.459
13	55	0.06	0.5	16.345	46.61	39.805	0.366
14	55	0.06	0.75	37.32	71.32	68.09	0.418
15	55	0.06	1	61.335	90.375	104.685	0.479
16	55	0.08	0.5	17.065	52.48	48.01	0.381
17	55	0.08	0.75	38.065	80.96	84.805	0.438
18	55	0.08	1	66.3	105.745	119.05	0.498
19	70	0.04	0.5	13.84	35.285	25.29	0.372
20	70	0.04	0.75	32.025	60.46	52.925	0.425
21	70	0.04	1	50.73	71.575	76.225	0.482
22	70	0.06	0.5	14.62	46.15	32.37	0.37
23	70	0.06	0.75	33.165	63.63	58.53	0.444
24	70	0.06	1	58.545	84.685	86.355	0.504
25	70	0.08	0.5	16.63	50.885	42.685	0.385
26	70	0.08	0.75	35.135	73.79	84.325	0.49
27	70	0.08	1	58.545	89.81	117.08	0.548

The purpose of the analysis of variance (ANOVA) is to find which design parameters significantly affect quality characteristic. The results of the analysis of variance (ANOVA) at a 5% level of significance for flank-wear, F_X, F_Y and F_Z are shown in Table 4.

Table 4. Result of analysis of variance (ANOVA) for VB, F_X, F_Y and F_Z.

Symbol	Degree of Freedom	Sum of Square	Mean Square	F	*p* Value	Contribution (%)	Remarks
ANOVA for VB							
V	2	0.0119094	0.0059547	49.69	0.000	14.02	Significant
f	2	0.0067667	0.0033834	28.23	0.000	7.96	Significant
d	2	0.0635050	0.0317525	264.95	0.000	74.78	Significant
v × f	4	0.0006750	0.001688	1.41	0.315	0.794	Not Significant
v × d	4	0.0008415	0.0002104	1.76	0.231	0.990	Not Significant
f × d	4	0.0002635	0.000659	0.55	0.705	0.310	Not Significant
Error	8	0.0009587	0.0001198			1.121	
Total	26	0.0849199					
ANOVA for F_X							
V	2	223.66	111.83	22.87	0.000	2.22	Significant
f	2	173.07	86.54	17.70	0.001	1.73	Significant
d	2	9463.08	4731.54	967.82	0.000	94.22	Significant
v × f	4	5.09	1.27	0.26	0.895	0.05	Not Significant
v × d	4	102.14	25.54	5.22	0.023	1.016	Significant
f × d	4	36.98	9.24	1.89	0.206	0.36	Not Significant
Error	8	39.11	4.89			0.38	
Total	26	10,043.14					
ANOVA for F_Y							
V	2	695.36	347.68	63.2	0.000	6.41	Significant
f	2	1155.87	577.94	105.07	0.000	10.65	Significant
d	2	8801.33	4400.67	800.12	0.000	81.15	Significant
v × f	4	11.38	2.85	0.51	0.726	0.105	Not Significant
v × d	4	92.68	23.17	4.212	0.040	0.85	Significant
f × d	4	44.70	11.17	2.030	0.183	0.412	Not Significant
Error	8	44.08	5.51			0.4057	
Total	26	10,845.4					
ANOVA for F_Z							
V	2	705.2	352.59	36.82	0.000	3.058	Significant
f	2	3723.3	1861.64	194.42	0.000	1.616	Significant
d	2	17,948.3	8974.14	937.2	0.000	77.84	Significant
v × f	4	67.1	16.78	1.75	0.231	0.291	Not Significant
v × d	4	62.3	15.58	1.627	0.258	0.2701	Not Significant
f × d	4	474.7	118.68	12.39	0.002	2.058	Significant
Error	8	76.6	9.575				
Total	26	23,057.5					

3.1. Main Effects Plot for VB, F_X, F_Y and F_Z

The main effects plot for VB is given in Figure 2a. From the figure, it is found that flank-wears i.e., wear of the flank, generally increases linearly with an increase in cutting speed, depth of cut and feed rate. The main effects plot for F_X is given in Figure 2b. From this figure, it is found that axial force generally decreases by increasing the cutting speed, but increases by increasing the feed rate and depth of cut. The main effects plot for F_X is given in Figure 2c. From this figure, it is found that radial force generally decreases by increasing the cutting speed, but increases by increasing the feed rate and depth of cut. The main effects plot for F_Y is given in Figure 2d. From this figure, it is found that the tangential cutting force generally decreases by increasing the cutting speed, but increases by increasing the feed rate and depth of cut.
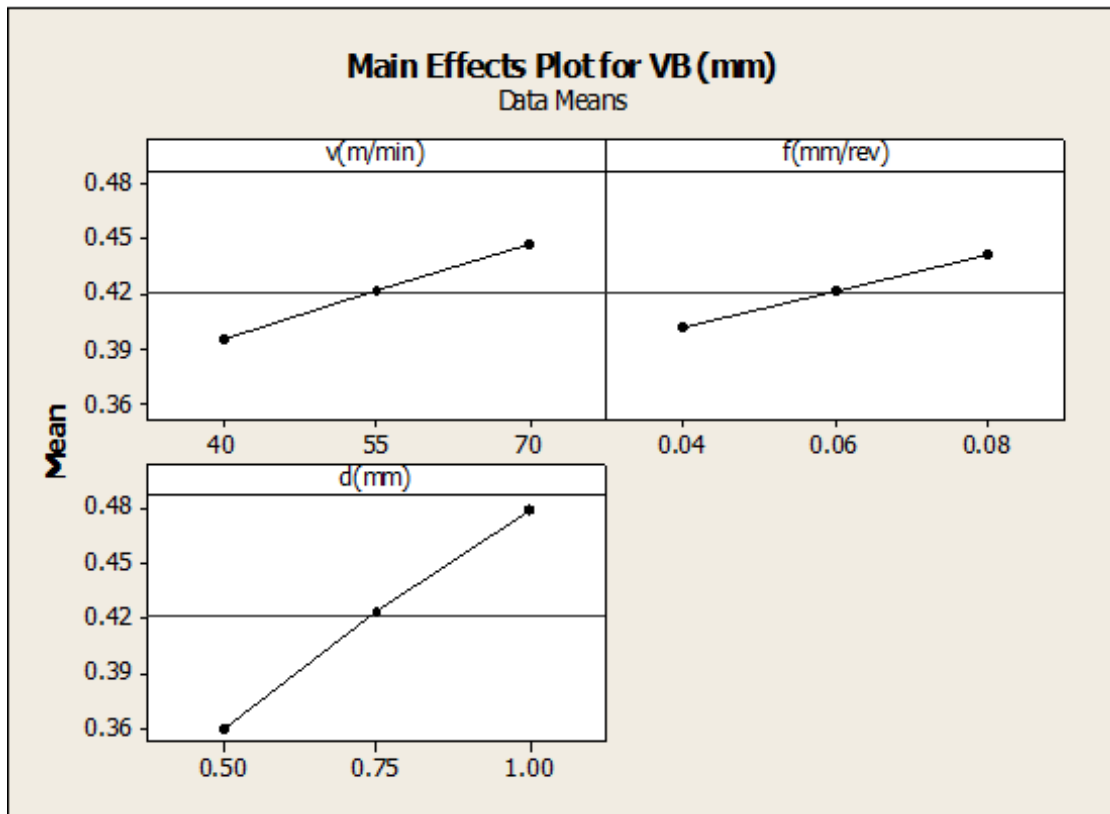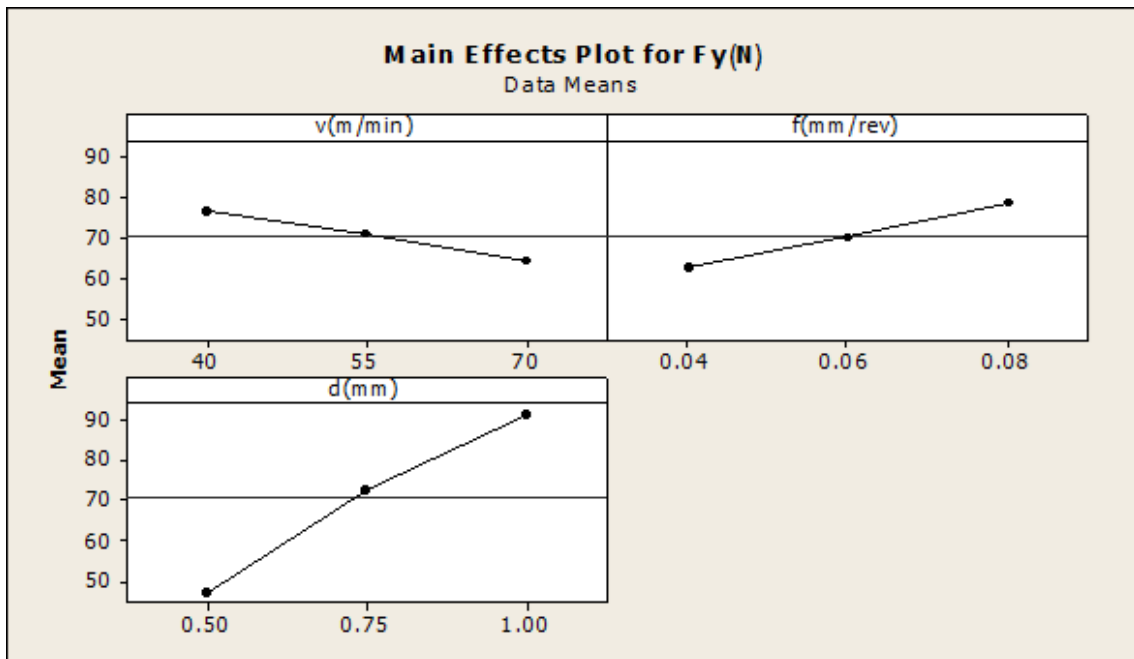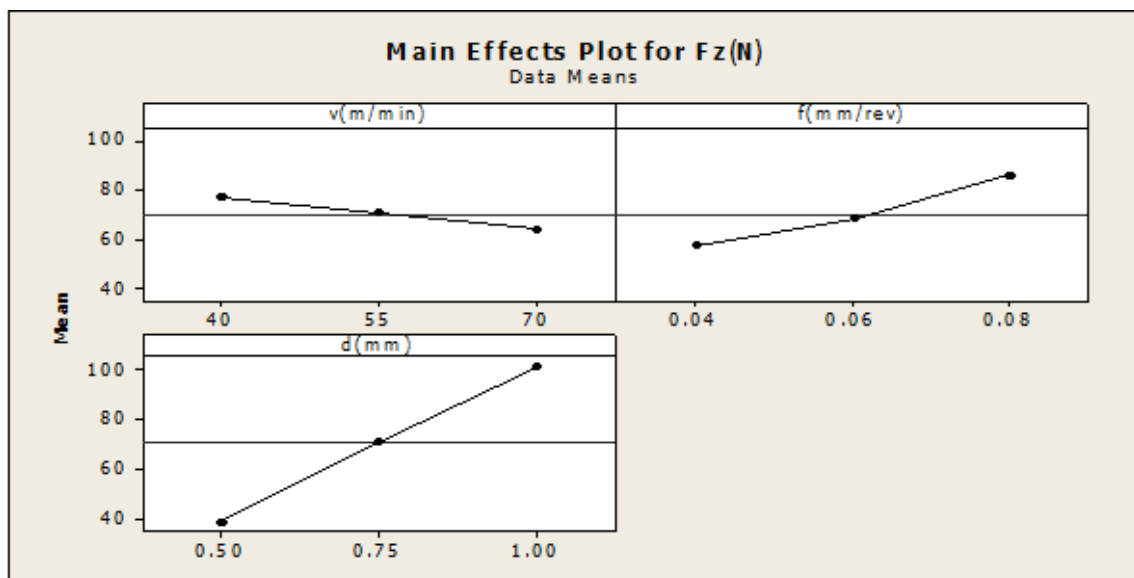
(**a**) Main Effects plot for VB
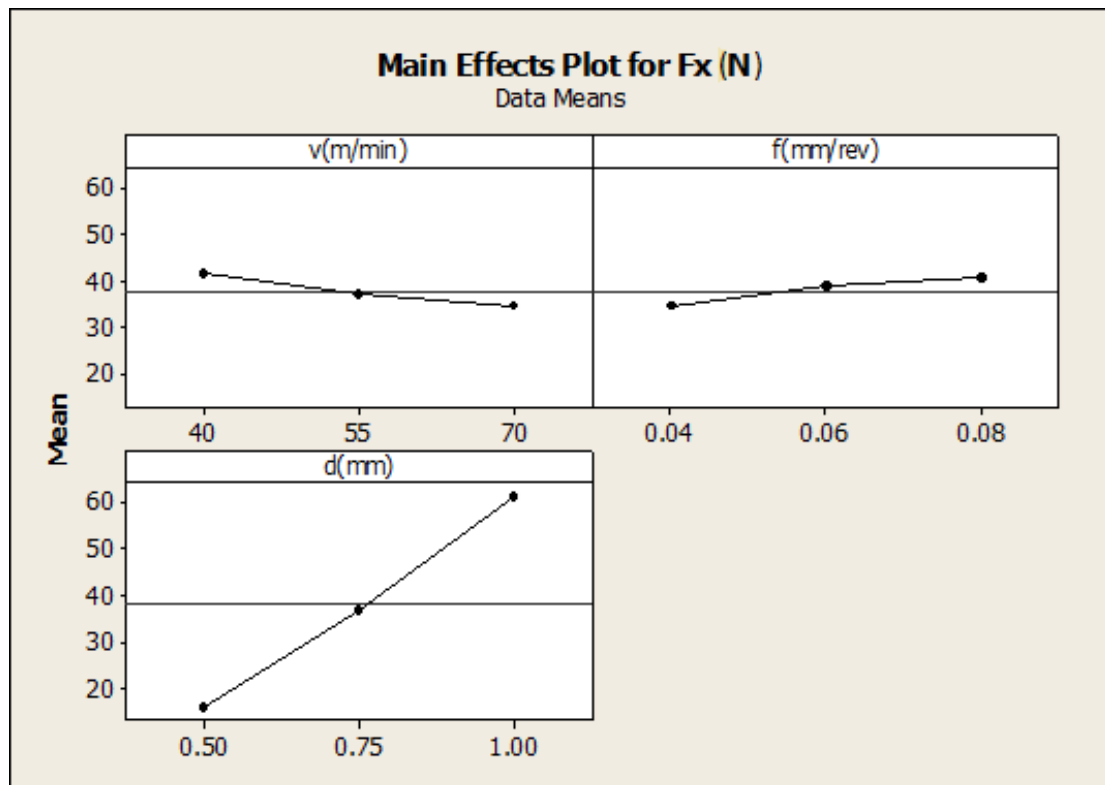
(**b**) Main Effects plot for Fx

Figure 2. *Cont.*

(**c**) Main Effects plot for F_Y

(**d**) Main Effects plot for F_Z

Figure 2. Main Effects Plot for VB, F_X, F_Y and F_Z.

3.2. Contour Plot for VB, F_X, F_Y and F_Z

The pair of input variables with the same response value can be represented by a pair of straight lines or contour lines. The contour plot of the VB is shown in Figure 3: (f × v), shows how the variables feed rate and cutting speed, are related to the VB. The constant value, i.e., the high-value one, was used for the depths of cut, (d). In the upper right-hand corner of the graph, i.e., in the darkest region, the highest value of the response is 0.52.
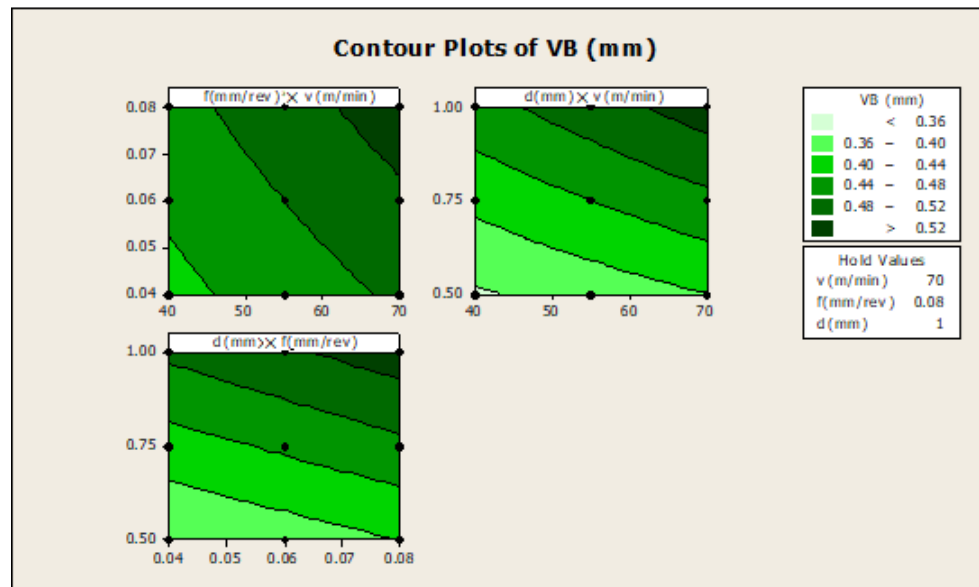
Figure 3. Contour plots for VB.

Figure 3: (d × v), the plot shows how the variables depth of cut and cutting speed, are related to the VB, while other factors such as feed rate are held constant, at a highest value of 0.08. In the upper right-hand corner of the graph, i.e., in the darkest region, the highest value of the response is greater than 0.52. In (d × f), the plot gives information of how variables such as depth of cut and feed rate are related to the VB, while other factors such as cutting speed are held constant, at a high value of 70.

In Figure 4 (f × v), the plot indicates how variables such as feed rate and cutting speed are related to the F_X, while other factors such as depth of cut (d) are held constant, at a high value of 1. The response is at its highest (greater than 70) in the darkest region of the graph (the upper left-hand corner). In (d × v), the plot indicates how variables such as depth of cut and cutting speed are related to the F_X, while others such as the feed-rate factor are held constant, at a high value of 0.08. The response is at its highest (greater than 70) in the darkest region of the graph (the upper left-hand corner). In (d × f), the plot indicates how variables, such as depth of cut and feed rate are related to the Fx while other factors such as cutting speed are held constant, at a high value of 70. The response is at its highest (between 50 and 60) in the dark region of the graph (the uppermost corner).
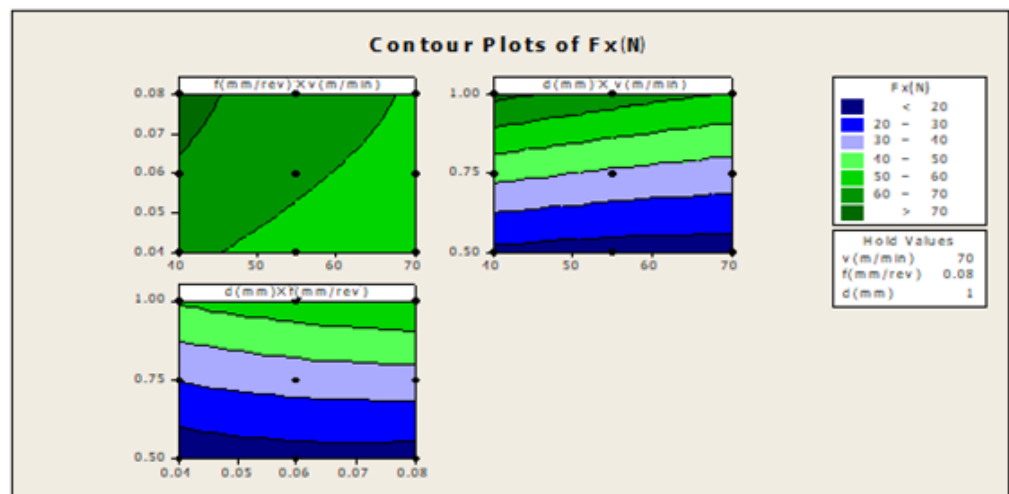

Figure 4. Contour plot for Fx.

Figure 5: (f × v)—the plot indicates how variables such as feed rate and cutting speed are related to the Fy, while other factors such as depth of cut (d) are held constant, at a high value of 1. The response is at its highest (greater than 100) in the darkest region of the graph (the upper left-hand corner); (d × v)—this plot indicates how variables such as depth of cut and cutting speed are related to the Fy, while other factors such as feed rate are held constant, at a high value of 0.08. The response is at its highest (greater than 100) in the darkest region of the graph (the upper left-hand corner); (d × f)—this plot indicates how variables such as depth of cut and feed rate are related to the Fy, while other factors such as cutting speed are held constant, at a high value 70. The response is at its highest (greater than 100) in the dark region of the graph (the upper right-hand corner).
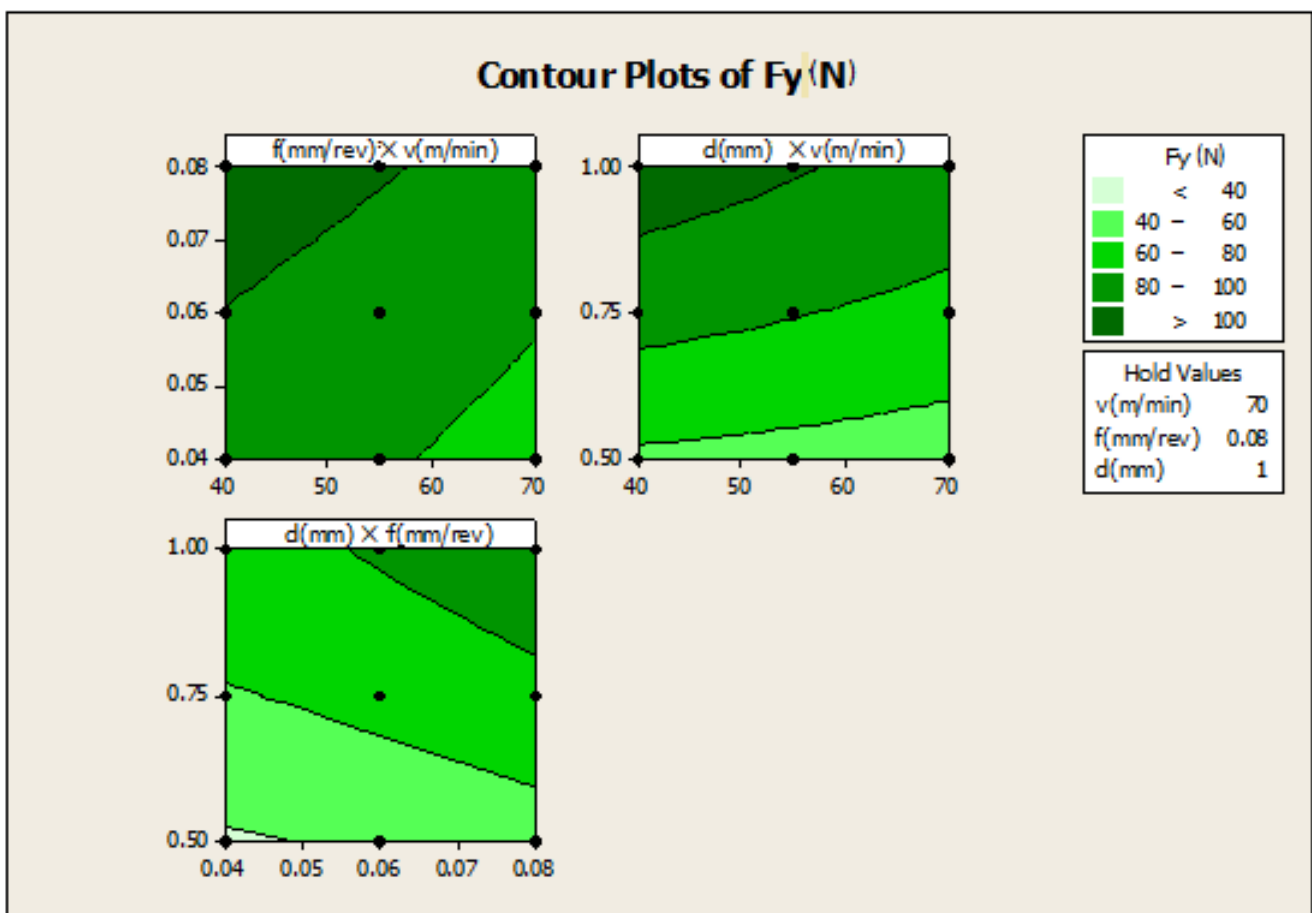

Figure 5. Contour plot for Fy.

In Figure 6, (f × v) the plot indicates how variables such as feed rate and cutting speed are related to the Fz, while other factors such as depth of cut (d) are held constant, at a high value of 1. The response is at its highest (greater than 120) in the darkest region of the graph (the upper left-hand corner); (d × v)—this plot indicates how variables such as depth of cut and cutting speed are related to the F_Z, while other factors such as feed rate are held constant, at a high value 0.08. The response is at its highest (greater than 120) in the darkest region of the graph (the upper left -hand corner); (d × f)—this plot indicates how variables, depth of cut and feed rate are related to the F_Z, while other factors such as cutting speed are held constant at a high value of 70. The response is at its highest (greater than 120) in the dark region of the graph (the upper right-hand corner).
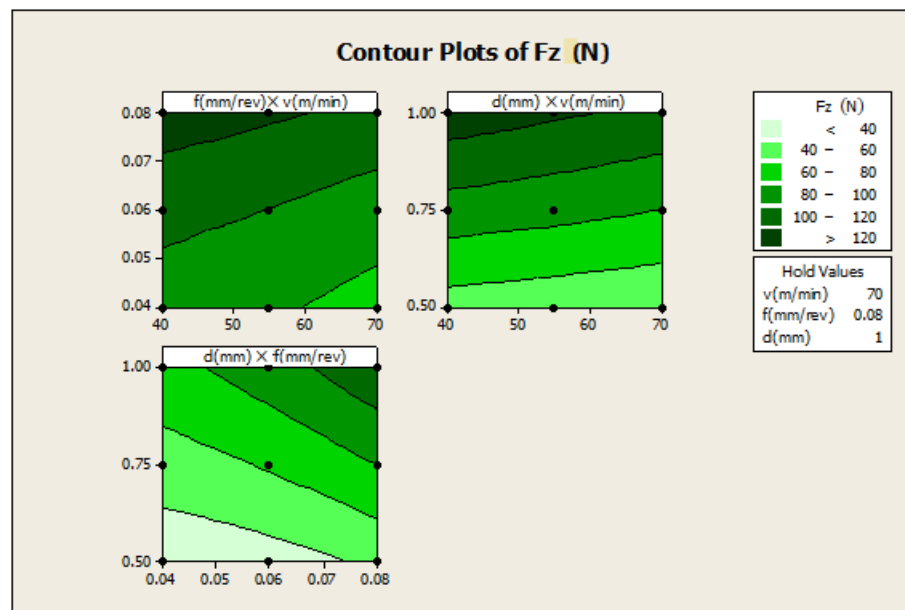
Figure 6. Contour plot for Fz.

3.3. Surface Plot for VB

The aim of this work is to understand the variation in the response in a particular direction, by changing the design variables. Generally, the response surface is a graphical representation, and with the help of a graph, the response can be visualised. The shape of the response surface, i.e., the ridgelines, valleys, and hills, can be visualised with the help of the graph. One can draw a three-dimensional plot for better understanding, and the side view shows the response surface. This type of plot is known as the response-surface plot. Hence, a clear snap of the response surface can be obtained with the help of a three-dimensional surface plot. The surface plot for VB is shown in Figures 7–10.
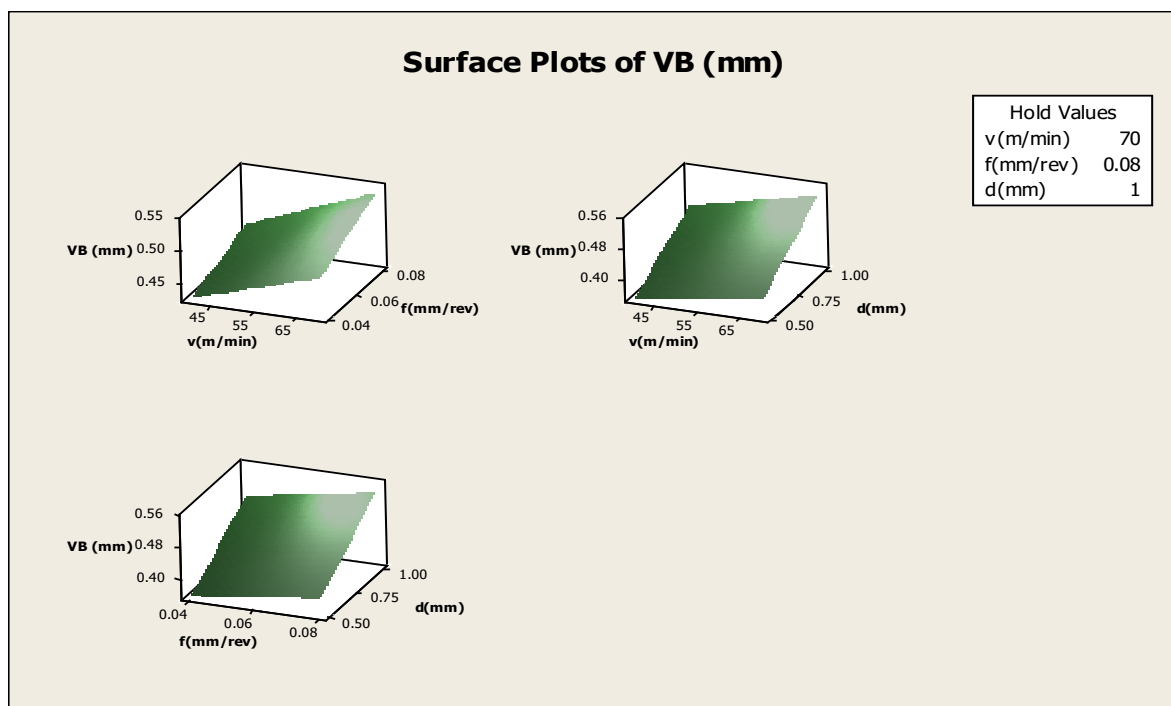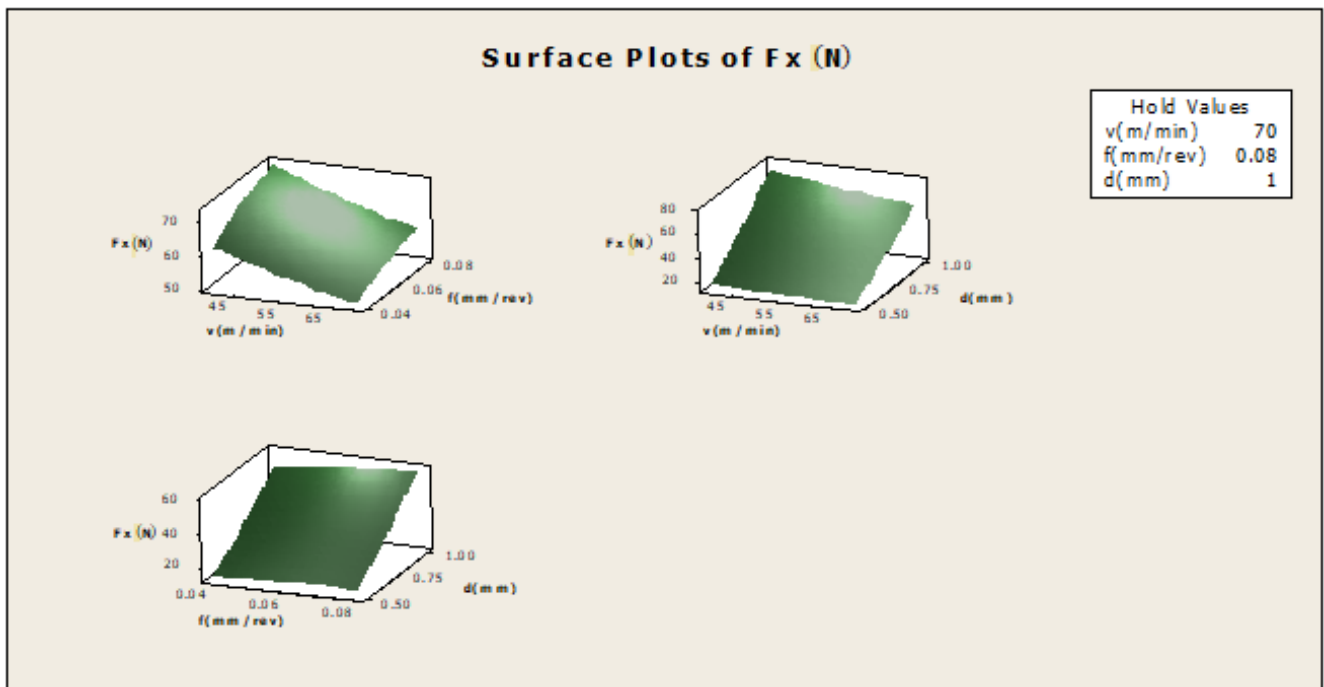

Figure 7. Surface plots for flank-wear.
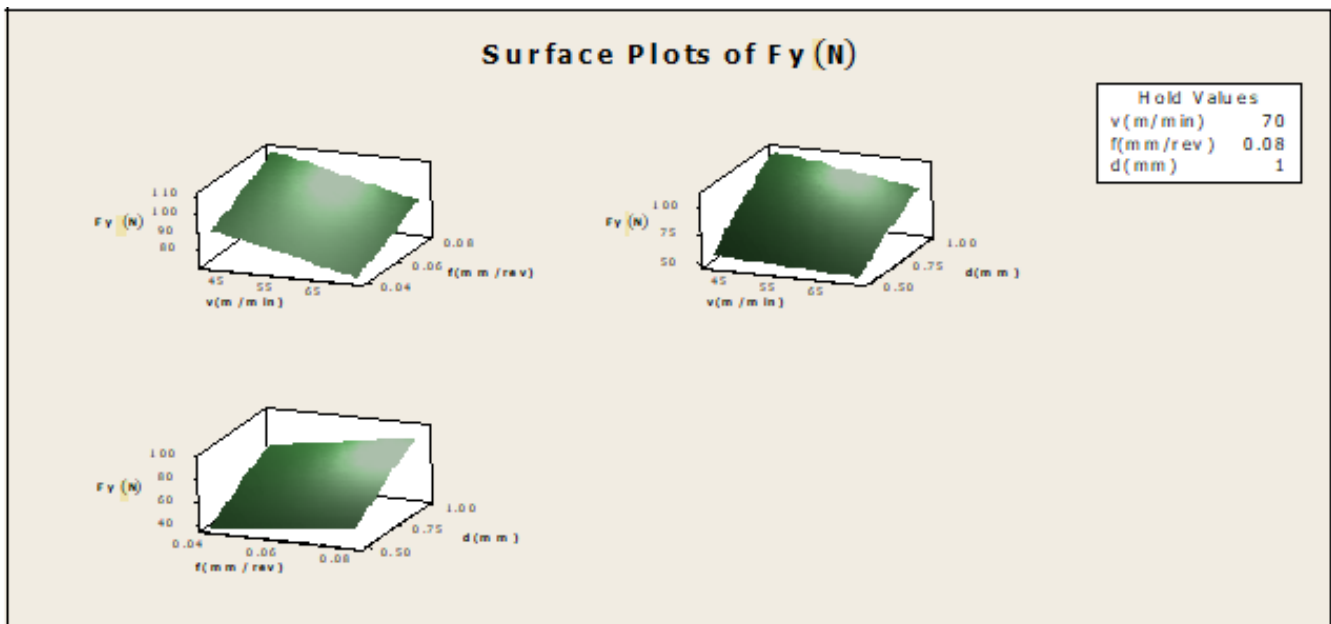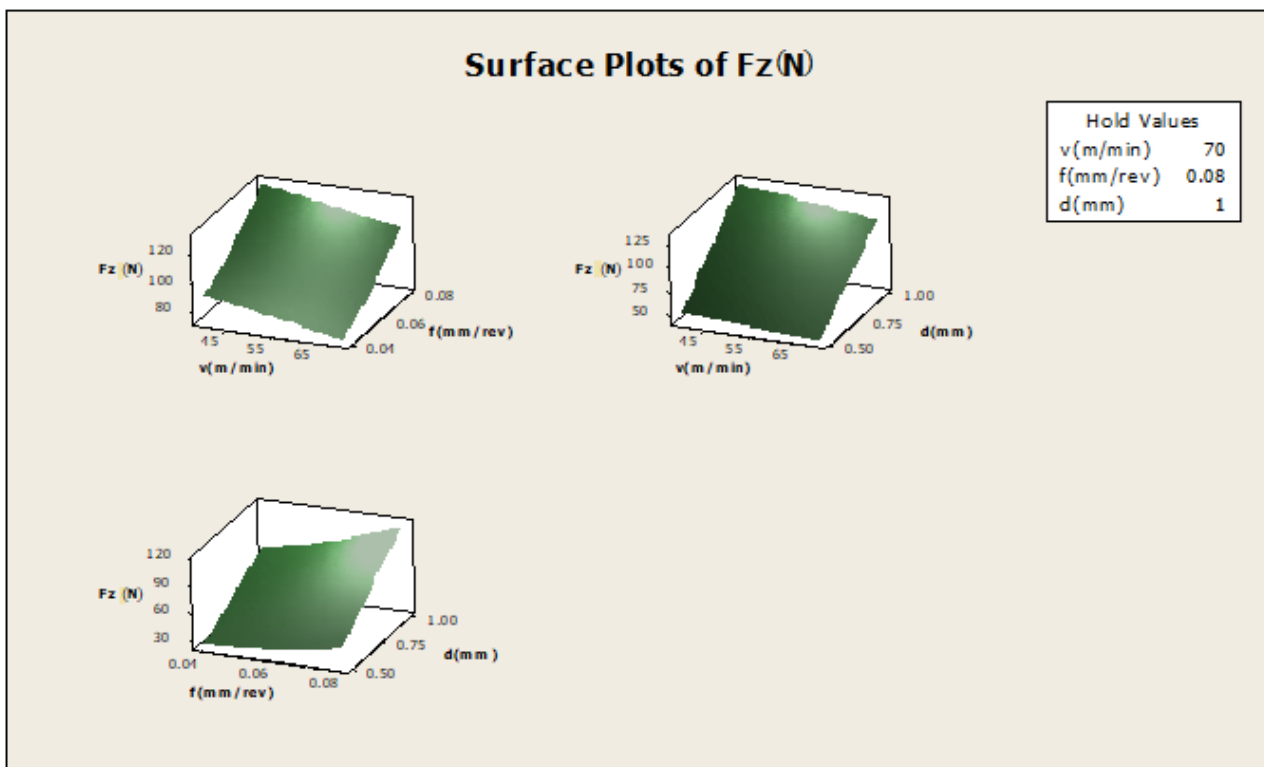
Figure 8. Surface plot for Fx.

Figure 9. Surface plot for F_Y.

Figure 10. Surface plot for F_Z.

3.4. Modelling of VB, F_X, F_Y and F_Z

The coefficient of correlation (R^2) was used to estimate the relevance and validity of the obtained results. An R^2 value shows how well the estimated model fits the data. The range of the values of R^2 is $0 \leq R^2 \leq 1$. For better fitting of the experimental data with the regression equation, the value of R^2 should be near 1. We used a linear regression analysis to fit the data. The VB model is given by the mathematical expression, and it can be expressed by Equation (1):

$$VB = 0.0904 + 0.00171\ v\ (m/min) + 0.969\ f\ (mm/rev) + 0.237\ d\ (mm) \tag{1}$$

Its coefficient of correlation, R^2 (adj.) is 96.33%. The main aim is to check whether this model is accurate or not. To do this, separate experiments were performed and their results were compared for predicted and measured values. We found that the predicted value of VB is almost nearer to the measured value. Hence, we can say that Equation (1) represents the data with 96.33% accuracy.

The F_X model is given by:

$$Fx = -49.48 + 0.441v + 6.889f + 113.84d - 0.757v \times d \tag{2}$$

The coefficient of the correlation R-sq. (adj) is 98.73%. We found that the predicted value of F_X was almost nearer to the measured value, which is shown in Figure 11a. Equation (2) shows a data accuracy of 98.73%.

The Fy model is given by:

$$Fy = -12.001 + 0.139v + 157.729f + 107.21d - 0.718v \times d \tag{3}$$

The coefficient of the correlation R-sq. (adj) is 98.68%. We found that the predicted value of F_Y was almost nearer to the measured value, which is shown in Figure 11b with 98.68% accuracy.
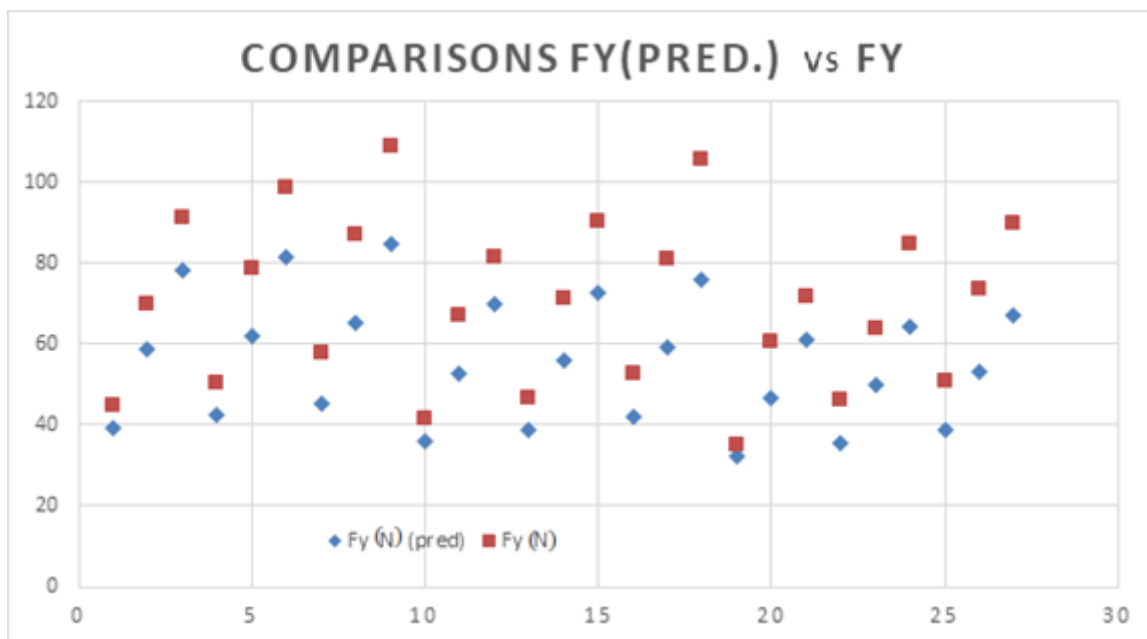
The Fz model is given by:

$$Fz = -9.47 - 0.08v - 229.14f + 84.07d + 1188f \times d \qquad (4)$$

The coefficient of the correlation R-sq. (adj) is 98.92%. We analysed the fact that the predicted value of F_Z was in full agreement with the measured value, which is shown in Figure 11c, with 98.92% accuracy.
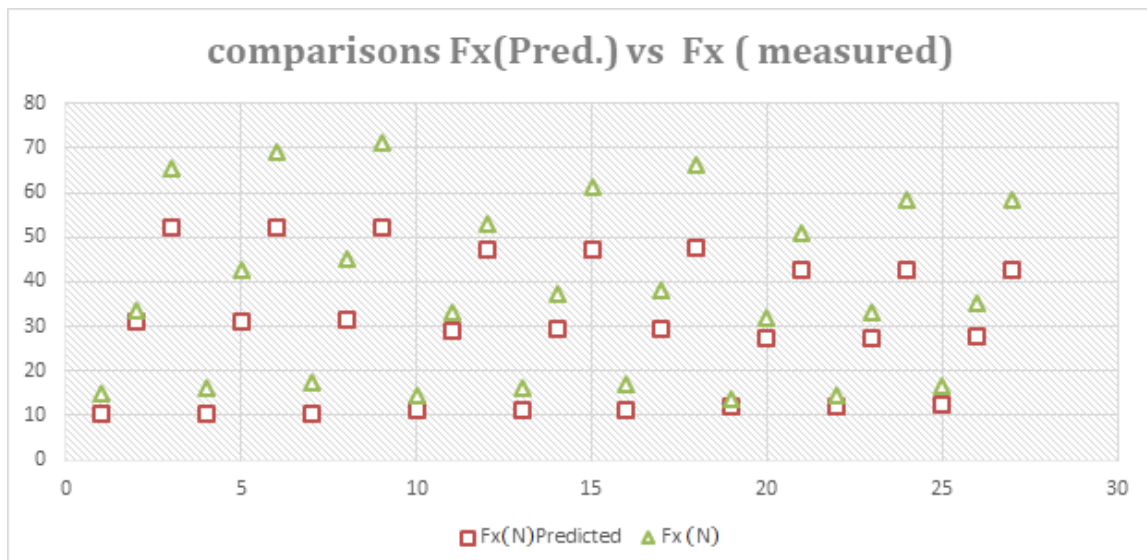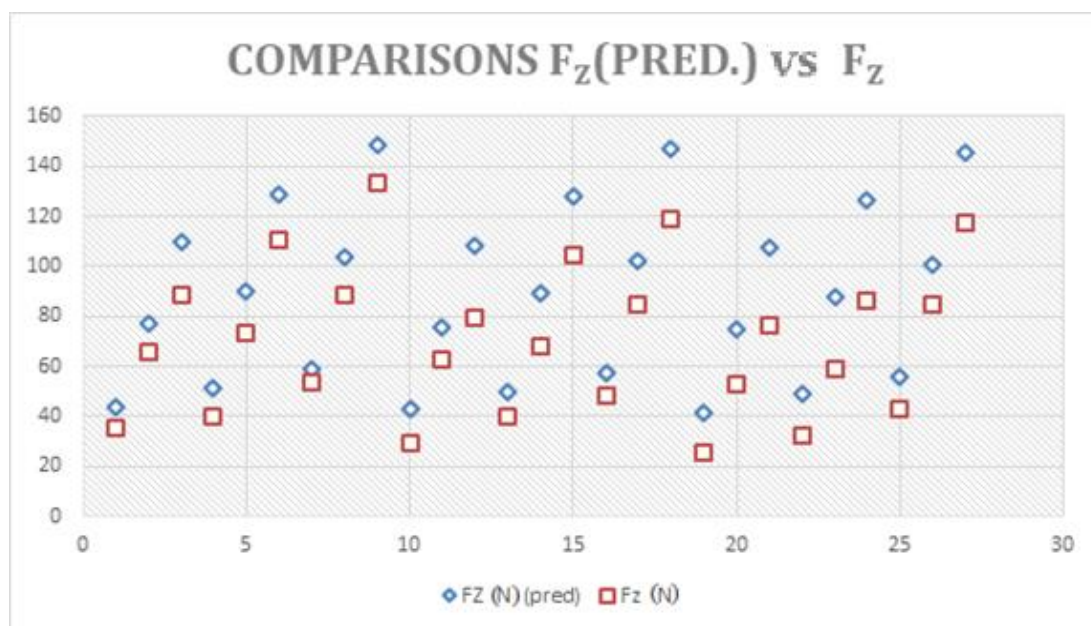

(**a**) Comparisons Fx (Pred.) vs. Fx (measured)

(**b**) Comparisons Fʏ (Pred.) vs. Fʏ (measured)

Figure 11. *Cont.*

(**c**) Comparisons Fz (Pred.) vs. Fz (measured)

Figure 11. Comparisons of predicated and measured values.

4. Conclusions

In the current study, a turning operation was performed on an EN36B steel work-billet with a tungsten carbide tool. The machining variables, i.e., the cutting speed and feed and depth of cut, were optimised to reduce the wear rate. The concept of response-surface methodology was used for designing this experiment. ANOVA and linear regression analysis were performed to linearly fit the experimental data. It was concluded that the cutting-force components (Fx, Fy and Fz) are governed by the depth of cut. It was also found that flank-wear, i.e., the wear of the flank, generally increases linearly by the increasing cutting speed, depth of cut and feed rate. A mathematical model was established to show the difference between predicted flank-wear and the actual flank wear in the experiment; it was revealed that the predicted value of the flank-wear was almost nearer to the measured value, with a 96.33% to 98.92% confidence level.

In the future, this research work can be extended to optimize the values of surface roughness and material-removal rate (MRR), by varying the machining parameters. Artificial Neural Network and other optimization techniques can be used to investigate the thermal contact conductance and heat transfer phenomenon between cutting tools and material surface [49–53].

Author Contributions: The main contributions of authors are as follows: conceptualization: R.K., S.B., A.K. and A.P.; methodology: L.K., C.S.M., A.G., A.K., A.P. and V.P.S.; structuring of paper: A.K., S.B., C.S.M., V.P.S., A.G. and A.P.; investigation and data collection: R.K., L.K., A.K. and C.S.M.; resources: R.K., L.K. and A.K.; data curation: A.K. and A.G.; writing—original draft: R.K., A.K., C.S.M. and A.P.; writing—review and editing: A.K., A.G., L.K. and A.P.; visualization: A.G. and C.S.M.; supervision: A.G., C.S.M. and R.K.; project administration: R.K. and L.K. All authors have read and agreed to the published version of the manuscript.

Institutional Review Board Statement: Not applicable.

Informed Consent Statement: Not applicable.

Data Availability Statement: Not applicable.

Conflicts of Interest: The authors declare no conflict of interest.

References

1. Choudhury, S.K.; Rath, S. In-process tool wear estimation in milling using cutting force model. *J. Mater. Process. Technol.* **2000**, *99*, 113–119. [CrossRef]
2. Davim, J.P.; Mata, F. Optimisation of surface roughness on turning fibre-reinforced plastics (FRPs) with diamond cutting tools. *Int. J. Adv. Manuf. Technol.* **2005**, *26*, 319–323. [CrossRef]
3. Elangovan, M.; Devasenapati, S.B.; Sakthivel, N.R.; Ramachandran, K.I. Evaluation of expert system for condition monitoring of a single point cutting tool using principle component analysis and decision tree algorithm. *Expert Syst. Appl.* **2011**, *38*, 4450–4459. [CrossRef]
4. Joardar, H.; Das, N.S.; Sutradhar, G. An experimental study of effect of process parameters in turning of LM6/SiCP metal matrix composite and its prediction using response surface methodology. *Int. J. Eng. Sci. Technol.* **2011**, *3*, 132–141. [CrossRef]
5. John, R.; Lin, R.; Jayaraman, K.; Bhattacharyya, D. Modified Taylor's equation including the effects of fiber characteristics on tool wear when machining natural fiber composites. *Wear* **2021**, *468–469*, 203606. [CrossRef]
6. Koren, Y. Flank Wear Model of Cutting Tools Using Control Theory. *J. Manuf. Sci. Eng.* **1978**, *100*, 103–109. [CrossRef]
7. Bhoi, S.; Kumar, A.; Prasad, A.; Meena, C.S.; Sarkar, R.B.; Mahto, B.; Ghosh, A. Performance Evaluation of Different Coating Materials in Delamination for Micro-Milling Applications on High-Speed Steel Substrate. *Micromachines* **2022**, *13*, 1277. [CrossRef]
8. Motorcu, A.R. Tool life performances, wear mechanisms and surface roughness characteristics when turning austenised and quenched AISI 52100 bearing steel with ceramics and CBN/TiC cutting tools. *Indian J. Eng. Mater. Sci.* **2011**, *18*, 137–146. Available online: https://nopr.niscpr.res.in/handle/123456789/11682 (accessed on 1 November 2022).
9. Sikdar, S.K.; Chen, M. Relationship between tool flank wear area and component forces in single point turning. *J. Mater. Process. Technol.* **2002**, *128*, 210–215. [CrossRef]
10. Sun, S.; Brandt, M.; Mo, J.P.T. Evolution of tool wear and its effect on cutting forces during dry machining of Ti-6Al-4V alloy. *Proc. Inst. Mech. Eng. Part B J. Eng. Manuf.* **2014**, *228*, 191–202. [CrossRef]
11. Noordin, M.Y.; Venkatesh, V.C.; Sharif, S.; Elting, S.; Abdullah, A. Application of response surface methodology in describing the performance of coated carbide tools when turning AISI 1045 steel. *J. Mater. Process. Technol.* **2004**, *145*, 46–58. [CrossRef]
12. Oraby, S.E.; Hayhurst, D.R. Tool life determination based on the measurement of wear and tool force ratio variation. *Int. J. Mach. Tools Manuf.* **2004**, *44*, 1261–1269. [CrossRef]
13. Kumar, A.; Patil, P.P. FEA Simulation and RSM Based Parametric Optimization of Vibrating Transmission Gearbox Housing. *Perspect. Sci.* **2016**, *8*, 388–391. [CrossRef]
14. Yang, W.H.; Tarng, Y.S. Design optimisation of cutting parameters for turning operations based on the Taguchi method. *J. Mater. Process. Technol.* **1998**, *84*, 122–129. [CrossRef]
15. Özel, T.; Zeren, E. Determination of work material flow stress and friction for FEA of machining using orthogonal cutting tests. *J. Mater. Process. Technol.* **2004**, *153–154*, 1019–1025. [CrossRef]
16. Habak, M.; Lebrun, J.L.; Levet, D.B. Effect of the microstructure on the tool/chip tribological contact in hard turning of 100Cr6 bearing steel. In Proceedings of the 10th CIRP International Workshop on Modeling of Machining Operations, Atlanta, GA, USA, 19 May 1998.
17. Kumar, A.; Patil, P.P. FEA Simulation Based Performance Study of Multi-speed Transmission Gearbox. *Int. J. Manuf. Mater. Mech. Eng.* **2016**, *6*, 57–67. [CrossRef]
18. García-Martínez, E.; Miguel, V.; Martínez-Martínez, A.; Coello, J.; Naranjo, J.A.; Manjabacas, M.C. Optimization of the Dry Turning Process of Ti48Al2Cr2Nb Aluminide Based on the Cutting Tool Configuration. *Materials* **2022**, *15*, 1472. [CrossRef]
19. Kumar, A.; Jaiswal, H.; Ahmad, F.; Patil, P.P. Dynamic Vibration Characteristics Analysis of Truck Transmission Gearbox Casing with Fixed Constraint of Vehicle Frame Based on FEA. *Procedia Eng.* **2014**, *97*, 1107–1115. [CrossRef]
20. Katiyar, P.K.; Singh, P.K.; Singh, R.; Lava Kumar, A. Modes of failure of cemented tungsten carbide tool bits (WC/Co): A study of wear parts. *Int. J. Refract. Met. Hard Mater.* **2016**, *54*, 27–38. [CrossRef]
21. Sharman, A.R.C.; Aspinwall, D.K.; Dewes, R.C.; Bowen, P. Workpiece surface integrity considerations when finish turning gamma titanium aluminide. *Wear* **2001**, *249*, 473–481. [CrossRef]
22. Zhao, J.; Liu, Z.; Wang, B.; Hu, J.; Wan, Y. Tool coating effects on cutting temperature during metal cutting processes: Comprehensive review and future research directions. *Mech. Syst. Signal Process.* **2021**, *150*, 107302. [CrossRef]
23. Takeyama, H.; Murata, R. Basic Investigation of Tool Wear. *J. Eng. Ind.* **1963**, *85*, 33–37. [CrossRef]
24. García-Martínez, E.; Martínez-Martínez, A.; Manjabacas, M.C.; Miguel, V. Proposal of a combined experimental-simulation methodology for the evaluation of machining temperature in turning processes. *Measurement* **2022**, *189*, 110632. [CrossRef]
25. Kumar, A.; Patil, P.P. Modal Analysis of Heavy Vehicle Truck Transmission Gearbox Housing Made from Different Materials. *J. Eng. Sci. Technol.* **2016**, *11*, 252–266.
26. García-Martínez, E.; Miguel, V.; Martínez, A.; Naranjo, J.A.; Coello, J. Tribological characterization of tribosystem Ti48Al2Cr2Nb-coated/uncoated carbide tools at different temperatures. *Wear* **2021**, *484–485*, 203992. [CrossRef]
27. Priarone, P.C.; Klocke, F.; Faga, M.G.; Lung, D.; Settineri, L. Tool life and surface integrity when turning titanium aluminides with PCD tools under conventional wet cutting and cryogenic cooling. *Int. J. Adv. Manuf. Technol.* **2016**, *85*, 807–816. [CrossRef]

28. Ivchenko, O.; Ivanov, V.; Trojanowska, J.; Zhyhylii, D.; Ciszak, O.; Zaloha, O.; Pavlenko, I.; Hladyshev, D. Method for an Effective Selection of Tools and Cutting Conditions during Precise Turning of Non-Alloy Quality Steel C45. *Materials* **2022**, *15*, 505. [CrossRef]

29. Kaščák, J.; Gašpár, Š.; Paško, J.; Husár, J.; Knapčíková, L. Polylactic Acid and Its Cellulose Based Composite as a Significant Tool for the Production of Optimized Models Modified for Additive Manufacturing. *Sustainability* **2021**, *13*, 1256. [CrossRef]

30. Kumar, A.; Patil, P. Dynamic Vibration Analysis of Heavy Vehicle Truck Transmission Gearbox Housing Using FEA. *J. Eng. Sci. Technol. Rev.* **2014**, *7*, 66–72. [CrossRef]

31. Ivchenko, O.; Zhyhylii, D.; Zaloha, O.; Zaloga, V.; Dehtiarenko, O. Resolution of the Friction Coefficient of Adhesion Under Cutting. In *Advanced Manufacturing Processes*; Tonkonogyi, V., Ed.; InterPartner-2019—Lecture Notes in Mechanical Engineering; Springer: Cham, Switzerland, 2020; pp. 98–107.

32. Cao, H.; Liu, L.; Wu, B.; Gao, Y.; Qu, D. Process optimization of high-speed dry milling UD-CF/PEEK laminates using GA-BP neural network. *Compos. Part B Eng.* **2021**, *221*, 109034. [CrossRef]

33. Kumar, A.; Jaiswal, H.; Pandey, A.; Patil, P.P. Free Vibration Analysis of Truck Transmission Housing Based on FEA. *Procedia Mater. Sci.* **2014**, *6*, 1588–1592. [CrossRef]

34. Bansal, A.; Bhardwaj, H.K.; Sharma, V.K.; Kumar, A. Static and dynamic behavior analysis of Al-6063 alloy using modified Hopkinson bar. In *Additive Manufacturing in Industry 4.0: Methods, Techniques, Modeling and Nano Aspects*; Sharma, V.K., Kumar, A., Gupta, M., Kumar, V., Sharma, D.K., Sharma, S.K., Eds.; CRC Press: Boca Raton, FL, USA, 2022; Chapter 6; pp. 107–124. [CrossRef]

35. Tlhabadira, I.; Daniyan, I.A.; Machaka, R.; Machio, C.; Masu, L.; VanStaden, L.R. Modelling and optimization of surface roughness during AISI P20 milling process using Taguchi method. *Int. J. Adv. Manuf. Technol.* **2019**, *102*, 3707–3718. [CrossRef]

36. Sharma, V.K.; Kumar, V.; Joshi, R.S.; Kumar, A. Effect of REOs on tribological behavior of aluminum hybrid composites using ANN. In *Additive Manufacturing in Industry 4.0: Methods, Techniques, Modeling and Nano Aspects*; Sharma, V.K., Kumar, A., Gupta, M., Kumar, V., Sharma, D.K., Sharma, S.K., Eds.; CRC Press: Boca Raton, FL, USA, 2022; Chapter 9; pp. 153–168. [CrossRef]

37. Gori, Y.; Verma, R.P.; Kumar, A.; Patil, P. FEA Based Fatigue crack Growth Analysis. *Mater. Today Proceedings* **2021**, *46*, 10575–10581. [CrossRef]

38. Maruda, R.W.; Legutko, S.; Mrugalski, R.; Dębowski, D.; Wojciechowski, S. Analysis of Cutting Force and Power Under the Conditions of Minimized Cooling in the Process of Turning AISI-1045 Steel with the Use of the Parameter Space Investigation Method. In *Industrial Measurements in Machining*; Królczyk, G., Niesłony, P., Królczyk, J., Eds.; IMM 2019—Lecture Notes in Mechanical Engineering; Springer: Cham, Switzerland, 2020; pp. 151–162.

39. Kalchenko, V.; Kalchenko, V.; Sira, N.; Yeroshenko, A.; Kalchenko, D. Three-Dimensional Simulation of Machined, Tool Surfaces and Shaping Process with Two-Side Grinding of Cylindrical Parts Ends. In *Advanced Manufacturing Processes*; Tonkonogyi, V., Ed.; InterPartner-2019—Lecture Notes in Mechanical Engineering; Springer: Cham, Switzerland, 2020; pp. 118–127.

40. Patil, P.P.; Kumar, A. Dynamic Structural and Thermal Characteristics Analysis of Oil Lubricated Multi Speed Transmission Gearbox: Variation of Load, Rotational Speed and Convection Heat Transfer. *Iran. J. Sci. Technol. Trans. Mech. Eng.* **2017**, *41*, 281–291. [CrossRef]

41. Heisel, U. Cause Analysis of errors in FE prediction orthogonal cutting performances. In Proceedings of the 10th CIRP International Workshop on Modeling of Machining Operations, Rende, Italy, 27–28 August 2007; pp. 141–148.

42. Tebaldo, V.; Faga, M.G. Influence of the heat treatment on the microstructure and machinability of titanium aluminides produced by electron beam melting. *J. Mater. Process. Technol.* **2017**, *244*, 289–303. [CrossRef]

43. Patil, P.P.; Sharma, S.C.; Jaiswal, H.; Kumar, A. Modeling Influence of Tube Material on Vibration based EMMFS using ANFIS. *Procedia Mater. Sci.* **2014**, *6*, 1097–1103. [CrossRef]

44. Patil, P.; Sharma, S.C.; Paliwal, V.; Kumar, A. ANN Modelling of Cu Type Omega Vibration Based Mass Flow Sensor. *Procedia Technol.* **2014**, *14*, 260–265. [CrossRef]

45. Singh, V.P.; Jain, S.; Karn, A.; Kumar, A.; Dwivedi, G.; Meena, C.S.; Cozzolino, R. Mathematical Modeling of Efficiency Evaluation of Double-Pass Parallel Flow Solar Air Heater. *Sustainability* **2022**, *14*, 10535. [CrossRef]

46. Kumar, A.; Jaiswal, H.; Patil, P.P. Connecting Bolt Constraint Based Design Parametric Optimisation of Vibrating Transmission Gearbox Housing Using RSM. *World J. Model. Simul.* **2017**, *13*, 228–240.

47. Kumar, A.; Jaiswal, H.; Patil, P.P. Parametric Optimization of Vibrating Heavy Vehicle Medium Duty Transmission Gearbox Housing Using Response Surface Method. *Int. J. Veh. Struct. Syst.* **2017**, *9*, 149–153. [CrossRef]

48. Patil, P.; Gori, Y.; Kumar, A.; Tyagi, M.R. Experimental Analysis of Tribological Properties of Polyisobutylene Thickened Oil in Lubricated Contacts. *Tribol. Int.* **2021**, *159*, 106983. [CrossRef]

49. Paul, A.K.; Prasad, A.; Kumar, A. Review on artificial neural network and its application in the field of engineering. *J. Mech. Eng. PRAKASH* **2022**, *1*, 53–61. [CrossRef]

50. Kumar, A.; Rana, S.; Gori, Y.; Sharma, N.K. Thermal Contact Conductance Prediction Using FEM Based Computational Techniques. In *Advanced Computational Methods in Mechanical and Materials Engineering*; Kumar, A., Gori, Y., Dutt, N., Singla, Y.K., Maurya, A., Eds.; CRC Press: Boca Raton, FL, USA, 2022; Chapter 11; pp. 183–220. [CrossRef]

51. Meena, C.S.; Kumar, A.; Roy, S.; Cannavale, A.; Ghosh, A. Review on Boiling Heat Transfer Enhancement Techniques. *Energies* **2022**, *15*, 5759. [CrossRef]
52. Rana, S.; Kumar, A. FEA Based Design and Thermal Contact Conductance Analysis of Steel and Al Rough Surfaces. *Int. J. Appl. Eng. Res.* **2019**, *13*, 12715–12724.
53. Rana, S.; Kumar, A.; Gori, Y.; Patil, P. Design and Analysis of Thermal Contact Conductance. *J. Crit. Rev.* **2019**, *6*, 363–370.